X-RAY CONE BEAM TOMOGRAPHY WITH TWO TILTED CIRCULAR TRAJECTORIES

Philippe Rizo, Pierre Grangeat, Pascal Sire,
Patrick Le Masson, and Solange Delagenière

Laboratoire d'Electronique de Technologie et d'Instrumentation
Département Systèmes
Centre d'Etudes Nucléaires de Grenoble
85X Avenue des Martyrs
38041, Grenoble Cedex, FRANCE

INTRODUCTION

Recently 3-D cone-beam tomography has become of interest for the nondestructive evaluation of advanced materials. The main field of application in nondestructive testing is the evaluation of structural ceramics. Study of such materials implies high density resolution and high sensitivity to cracks. In fact, with a single circular source trajectory, when the cone-beam aperture increases, density is underestimated and cone shaped artifacts may appear at interfaces in the sample even at relatively small aperture [1-3]. These artifacts limit the thickness we can examine with a planar source trajectory. To maintain optimal reconstruction accuracy with a circular source trajectory, the angular aperture must remain within ±10°. However Kudo and Saito [4] showed that this limit can be slightly overcome by using a special interpolation of the shadow area. But to examine greater thicknesses and to maintain resolution, we must widen the cone-beam aperture thereby decreasing accuracy. To overcome these aperture limitations, Tuy [5] introduced the double circular source trajectory idea.

Until now, most of the experiments presented in the literature were performed with a planar source trajectory [1,2,3,4,6]. Recently, a new method presented by Smith [7,8] has been applied to nonplanar source trajectories by Kudo and Saito [9]. The inversion presented by Kudo uses the Hilbert transform of the first derivative of the Radon transform. This inversion has been experienced with real data on two circular trajectories at 90° with intersection of the two axis of the trajectories (orthogonal scan).

We have presented [10] reconstructions on simulated with double circular source trajectories with an exact reconstruction method using the inversion of the first derivative of the 3-D Radon transform. These simulations were performed with an angle smaller than 90° between the two trajectories. Here we quantify the advantages of this method and we present experimental reconstruction in this implementation. We show also that according to the Radon space sampling, the axes of the two trajectories do not have to intersect, but they must be close enough.

MATHEMATICAL BACKGROUND

Grangeat [11,12] showed that we can link exactly the X-ray transform of an object and the first derivative of its 3D Radon transform. Given an object function f(M) where M is a given point of the space, let us define the X-ray transform Xf(S,A), as the radiographic reading at point A corresponding to a source position S:

$$Xf\,(S,A) = \int_{a=0}^{+\infty} f\left(S + a.\vec{u'_1}\right)da \quad \text{with} \quad \vec{u'_1} = \frac{\vec{SA}}{\|\vec{SA}\|} \qquad (1)$$

Review of Progress in Quantitative Nondestructive Evaluation, Vol. 11
Edited by D.O. Thompson and D.E. Chimenti, Plenum Press, New York, 1992

where A is a point of the detection plane PX, which is a plane parallel to the detector passing through the origin O.

If we consider a plane P of normal vector $\vec{n}$, at a distance ρ of the origin O, the Radon transform of f on the plane P is given by :

$$Rf(\rho,\vec{n}) = \int_{M \in P(\rho,\vec{n})} f(M)\, dM \tag{2}$$

In the Radon space the characteristic point C of the plane P is defined by $\vec{OC} = \rho\,\vec{n}$.

We call $SYf(S,\vec{n})$ the integral over the line $D(S,\vec{n})$ intersecting the detector and the plane passing through S and perpendicular to $\vec{n}$ (see Fig. 1):

$$SYf(S,\vec{n}) = \int_{A \in D(S,\vec{n})} Yf(S,A)\, dA \tag{3}$$

where:

$$Yf(S,A) = \frac{\|\vec{SO}\|}{\|\vec{SA}\|} \,.\, Xf(S,A) \quad , \quad A \in PX \tag{4}$$

Then the Grangeat formula can be written as:

$$\frac{\|\vec{OS}\|^2}{\|\vec{OS} \wedge \vec{n}\|^2} \,.\, \frac{\partial SYf}{\partial \rho'}(S,\vec{n}) = R'f(\vec{OS}.\vec{n}, \vec{n}) \tag{5}$$

where ρ' is the distance from the origin O to the detection line $D(S,\vec{n})$, (see Fig. 1). Once the first derivative of the 3D Radon transform is filled, it is inverted by two sets of backprojections.

$$f(M) = -\frac{1}{8\pi^2} \,.\, \int_{S^2} \frac{\partial^2 Rf}{\partial \rho^2}(\vec{OM}.\vec{n},\vec{n})\, d\vec{n} \tag{6}$$

We see (Fig. 1) that for each source position, the set of C points defines a sphere in the 3D Radon space. This set of points of the 3D Radon space that can be described by a circular source trajectory is a torus [2,9,11,12].

METHOD

Kirillov[13] and Tuy[5] showed that in order to perform exact 3-D cone-beam tomography, all planes passing through each point of the object must cut the source trajectory at least once. Obviously, in the case of the circular trajectory, the planes that are parallel to the trajectory and cross the sample do not follow this condition (Fig. 2). Thus, no information lying in these planes is detected. The principle of double circular source trajectories is to define a second trajectory that sees the undetected planes with the first trajectory (Fig. 3). Assuming that the first trajectory has a source to rotation axis distance equal to rsou1 and the second trajectory a source to rotation axis distance of rsou2, if ξ is the angle between the two trajectories, the maximum object diameter Rrad that can be reconstructed following the above conditions is:

$$Rrad = \frac{rsou1.rsou2.\sin\xi}{\sqrt{rsou2^2 + 2.rsou2.rsou1 + rsou1^2}}$$

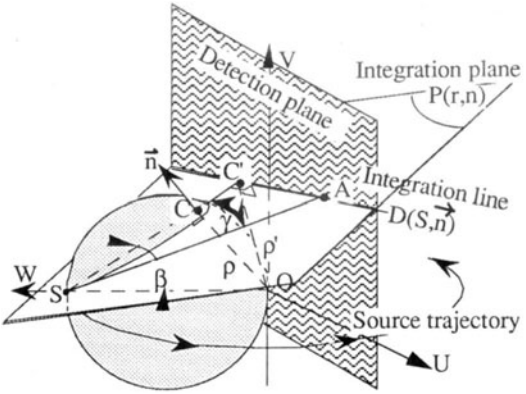

Fig. 1. Definition of the acquisition geometry. The X-rays are emitted at S and produce a radiograph of the object on the detection plane. Each projection defines a sphere in the radon space.

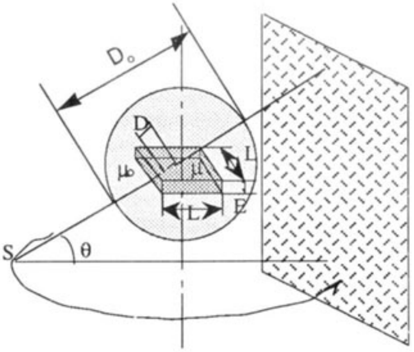

Fig. 2. Detectability of horizontal features. If θ=0 the defect is in the cental slice, D=L and the defect is detected. If θ ≠0 the deffect may not be detected, D=E/sin(θ) the defect will be detected only if E is large enough.

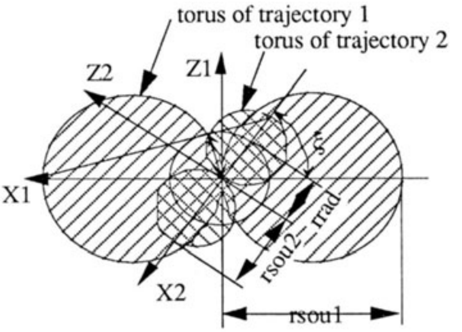

Fig. 3. Maximum radius of the examined object with double circular trajectory. The radii of the trajectories are rsou1 and rsou2 and the angle between the trajectories is ξ

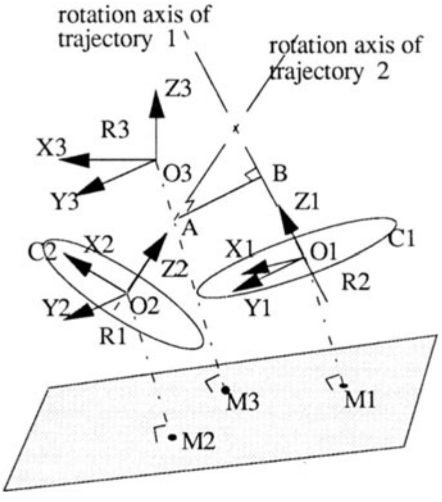

Figure 4. Principle of the change of coordinates in 3D-Radon spaces.

For each trajectory, we compute the set of detected points of the Radon space in a coordinate system linked to the trajectory. To parametrize in a third coordinate system a complete Radon transform of the object space (Fig. 4), for each point of this space we compute the corresponding points in the other systems of coordinates. The value of the point M3 in the Radon space of origin O3 is the integral of the density value of the object over the plane passing through M3 and orthogonal to (O3,M3). The corresponding value in the space of origin O1 and O2 will be given by the value of the orthogonal projection M1 and M2 of the points O1 and O2 on the plane defined by M3. If M1 and M2 are within the intersection domain of the two torus of the measurements sets 1 and 2 (Fig.3), we average the two values. If M1 is in the shadow area of space 1 then M2 should not be in the shadow area of space 2, thus we give to M3 the value of M2 (and respectively). For reconstruction, the 3D Radon transform is expressed in spherical coordinates (ρ,θ,φ) sampled with a sampling rate of Perho, Peteta, Pephi. Therefore the misalignment of the two trajectories does not produce missing information if the distance between the two centers of trajectories is smaller than Perho.

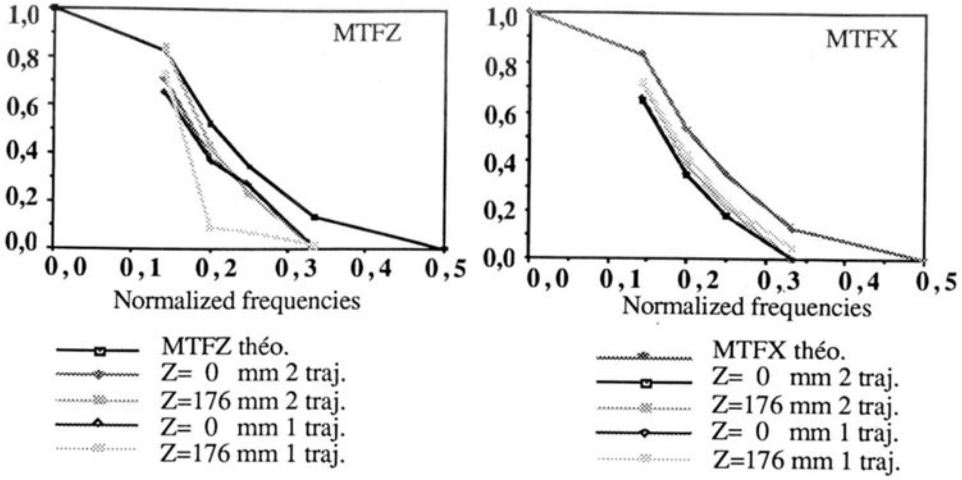

Fig. 5. Modulation transfer function measurements

MODULATION TRANSFER FUNCTION MEASUREMENTS

We initially introduced this method [2-14]. The principle is to use the reconstruction of a set of concentric spheres to measure the response of the reconstruction code to particular frequencies. Let us define h_C the local impulse response function in the neighborhood of the point C and fc an input of the system. We assume that the spread of this impulse response is sufficiently small with respect to the spatial distortions and to the spread of the test functions such that the following convolution relation is still valid at all points:

$$s_C = h_C * f_C \tag{7}$$

The local Modulation Transfer Function (MTF) is the 3D Fourier transform Fh_C of the impulse response h_C. To measure the MTF Fh_C, we have to compute the 3D Fourier transforms Fs_C and Ff_C for a given test function and to compute their ratio. We combine three uniform spheres $c_r(M)$ of radius r, 2r and 3r, to get the following test function :

$$f_{(O,r)}(M) = D \,.\, \left[c_r(M) - c_{2r}(M) + c_{3r}(M)\right] \tag{8}$$

where D is the attenuation value of this test function.

$f_{(O,r)}(M)$ has a spherical symmetry, so its 3D Fourier transform has a spherical symmetry. Let us denote $Ff_{(o,r)}(\nu)$ its radial variations. It is given by the following relation:

$$Ff_{(O,r)}(\nu)=\left(\frac{r}{\nu}\right)^{3/2}\left[J_{3/2}(2\pi\nu r)-2^{3/2}J_{3/2}(4\pi\nu r)+3^{3/2}J_{3/2}(6\pi\nu r)\right].D \tag{9}$$

where $J_{3/2}$ is a Bessel function of the first type. $Ff_{(O,r)}(\nu)$ is close to a maximum for $\nu=\frac{1}{2r}$.
We first show the axial variations MTFZ of the MTF, which means the variations along the rotation axis. To get this 3D Fourier transform, we integrate along axial planes the functions restricted to a limited volume V around the test function and we compute a 1D Fourier transform along the axial direction for the adapted frequency and with integration bounds restricted to the projection of V. Then we show the radial variations MTFX of the MTF.
We see on figure 5 the improvement on the MTFZ of the reconstruction even for aperture as small as 10°. This improvement is even more obvious at larger apertures. The MTFX is almost not perturbed by the vertical aperture.

LEVEL DISTORTIONS

To check the response of the reconstruction code at very low frequencies, like in [2,10] we placed a set of simulated uniform spheres on one of the rotation axis of the system, and we reconstructed it with the Feldkamp code and the Radon code with single circular source trajectory. For Radon, we present one case with linear interpolation of the shadow area and one without interpolation. Finally, we present the reconstruction with a double circular source trajectory.

We see in Figure 6 the underestimation of the attenuation coefficients at large apertures for whatever reconstruction algorithm used in single circular trajectory.The relative mean square error on the density can be as high as 20% at an aperture of ±30°. However, for the double circular trajectory reconstruction,the relative mean square error stay under 2%.

CONE SHAPED ARTEFACTS DUE TO THE SHADOW AREA

We show in this section the characteristic artifacts due to the missing information with single circular source trajectories and the suppression of these artifacts using a complete trajectory like a double circular trajectory. First we present the artifact supression on a set of simulated data with an orthogonal scan.Second we show the same improvement on experimental data.

Simulated data reconstructions

In this part we projected in two sets of circular trajectories at 90° (orthogonal scan) a 3D volume representing a lumbar vertebrae. The advantage of simulated data is to avoid alignment problems .

The acquisition geometry is the following:
source-axis distance = 116 mm
vertical sampling of the detector = 1.047 mm
horizontal sampling of the detector = 1.047 mm
number of projections = 240
The reconstruction geometry is the following:
vertical sampling of the object = 1.047 mm
horizontal sampling of the object = 1.047 mm
size of the reconstructed object = 64*64*64 pixels

Figures 8 and 9 show a surface displays of the same vertebrae reconstructed in single circular source trajectory with the 3D backprojection software (Feldkamp algorithm) [6] and with the Radon software (Grangeat algorithm)[12]. Figure 10 shows a surface display of the same vertebrae after reconstruction with Radon algorithm in double circular source trajectory. The three reconstructed volumes have the same normalization. We see that for suppressing reconstructions artifacts, we have to threshold the data at a very high level on the single circular source trajectory reconstructions. This means that the densities close to the edge of the sample are poorly reconstructed with a single source trajectory whatever the algorithm used. They are slightly overestimated along edges parallel to the source trajectory.

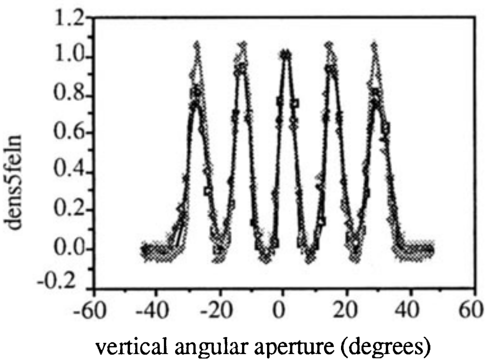

Fig. 6. Reconstruction of uniform spheres with the different cone-beam reconstruction codes.

—□— 3-D backprojection
·····◆····· Radon 2 axis
·····▨····· Radon 1 axis
—◇— Radon 1 axis 0. in shadow area

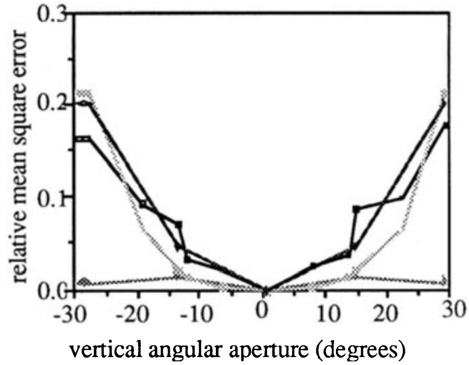

Fig. 7. Relative mean square error of the different cone-beam reconstruction codes.

—□— 3-D backprojection
·····◆····· Radon 2 axis
·····▨····· Radon 1 axis
—◇— Radon 1 axis 0. in shadow area

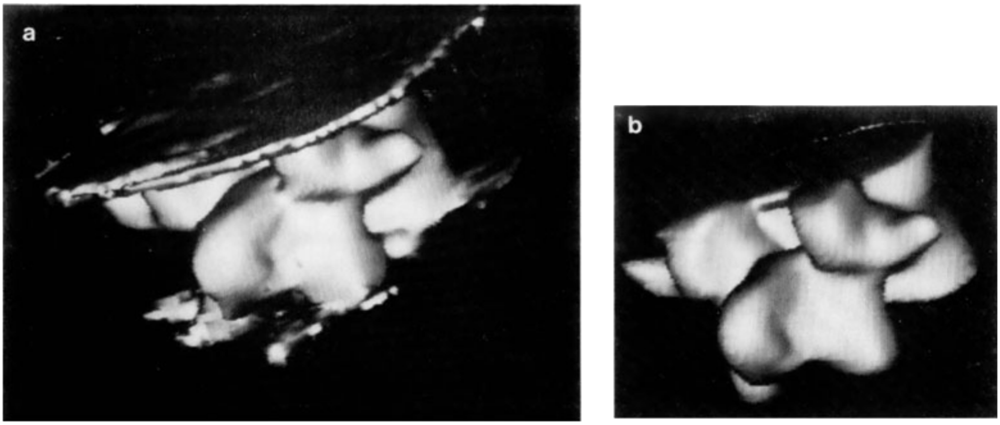

Fig. 8. Vertebrae reconstruction with 3D backprojection algorithm in single circular source trajectory . (a) density threshold at 7% of the maximum density value. (b) Density threshold at 9% of the maximum density value

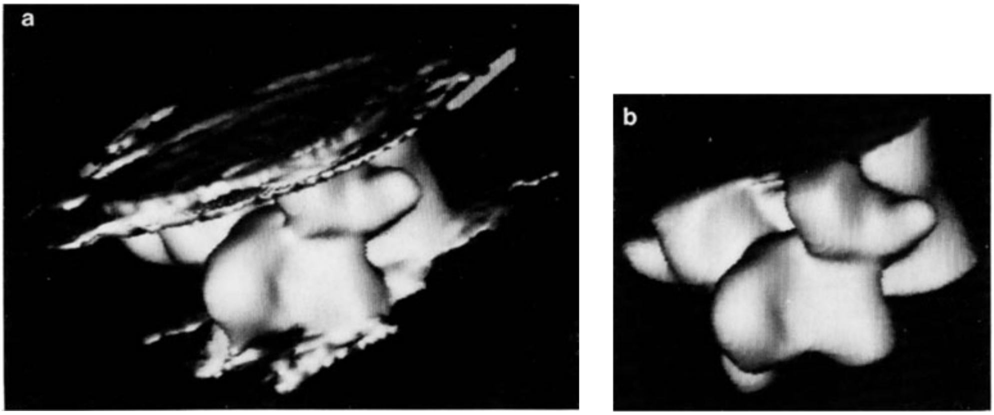

Fig. 9. Vertebrae reconstruction with Radon algorithm in single circular source trajectory . (a) density threshold at 5% of the maximum density value. (b) Density threshold at 7.5% of the maximum density value

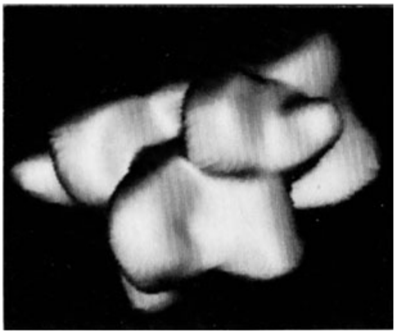

Fig. 10. Vertebrae reconstruction with 3D backprojection algorithm in double circular source trajectory and a density threshold at 2% of the maximum density value.

Experimental data reconstruction

The following results have been acquired on the experimental bench EVA devoted to structural ceramics examination [15]. This experimental system consist of a HOMX161 IRT microfocus X-ray source, a precise tri-field image intensifier, and a SOFRETEC CCD camera. The movements of the sample are controlled by a Microcontrôle precision manipulation stage driven by a PC. The PC is also linked to an IMAGING TECHNOLOGY series 150 system for frame grabbing and local image processing. After acquisition, data are sent from the PC memory to a VAX 6300 via a local area network. Then the reconstruction software, developed by Leti, are executed either on the VAX or on the Cray II. The obeserved object was a cylinder of aluminum on which we carved some grooves, therefore the density in the sample is supposed to be constant.

The acquisition geometry was the following:
source-axis distance =130.5 mm
vertical sampling of the detector = 0.49 mm
horizontal sampling of the detector = 0.69 mm
number of projections = 128

In the case of the double circular source trajectory reconstruction, the angle between the two trajectories was 40°.

The reconstruction geometry was the following:
vertical sampling of the object = 0.49 mm
horizontal sampling of the object = 0.69 mm
size of the reconstructed object = 64*64*64 pixels

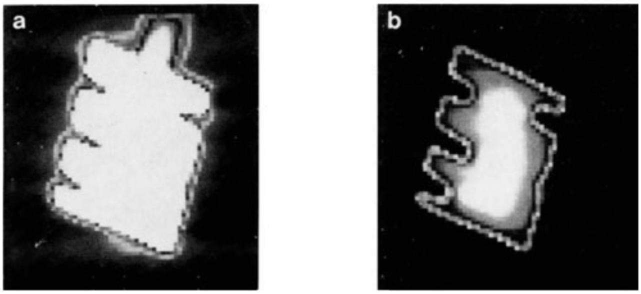

Fig. 11. Experimental reconstruction of an aluminum rod with Radon algorithm using single circular source trajectory . (a) Visualization of the artifacts outside the sample.we see strong horizontal artifacts on the edges of the sample. (b) Visualization of the artifacts in the sample. We notice the underestimation of the densities in the sample close to the edges.

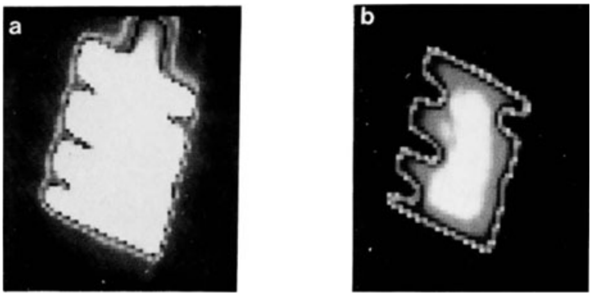

Fig. 12. Experimental reconstruction of an aluminum rod with Radon algorithm using double circular source trajectory . (a) visualization of the artifacts outside the sample. We see no horizontal artifacts on the edges of the sample. (b) Visualization of the artifacts in the sample. We notice homogenous densities in the sample close to the edges.

We see on figure 11 the almost horizontal artefact on the sample edges for the single circular source trajectory. These artifacts are completely suppressed in the double circular source trajectory. We see also on figure 12 that with the single circular source trajectory the density in the object close to the edges of the sample is not acurate, it is underestimated.

CONCLUSIONS

We have shown that 3-D cone-beam tomography with double circular source trajectory suppresses problems of missing information encountered with single circular trajectories.

With this reconstruction method, density resolution is independent of interest-area position, and streak artifacts characteristic of single circular trajectory reconstructions are suppressed.

This method can be implemented without approximation using the Grangeat formula.

We demonstrated with experimental acquisitions that such a method allows the design of 3-D cone-beam tomography scanners for evaluation of small components with accurate reconstructions.

ACKNOWLEDGEMENTS

We would like to thank Intercontrôle who provided the experimental bench EVA for the dual circular source trajectory experiment. This research was partly supported by the C.E.E. Brite project, contract GR-77.528 C.E.E.

REFERENCES

1. P. Rizo, P. Grangeat, in Proc. of the Industrial Computerized Tomography Conf. (Am. Soc. for Nondest Test., Seattle, 1989), 24-28
2. P. Rizo, P. Grangeat, P. Sire, P. Lemasson, P. Melennec, "Comparison of two 3D X-ray cone-beam reconstruction algorithms with circular source trajectory" J. of Opt. Soc. Oct 1991
3. P. Rizo, W. A. Ellingson, in Proc of the Nondestructive Evaluation of Ceramics Conf., (Am. Soc. for Nondest. Test., Columbus, OH, 1990), 121-125
4. H. Kudo, T. Saito, in Proc. Topical Meeting, O.S.A., Signal Recovery and Synthesis *III*, Cape Cod, MA, 1989, 174-177
5. H. K. Tuy, SIAM J. Appl. Math. 43 (3), 546-552 (1983)
6. L. A. Feldkamp, L. C. Davis, J. W. Kress, J. Opt. Soc. Am. 1 (6),612-619 (1984)
7. B. D. Smith, Ph. D. thesis, University of Rhode Island (1987)
8. B. D. Smith, IEEE Trans. Med. Imaging, MI-3, 91-98, (1984)
9. H.Kudo, T Saito, J. Opt. Soc. Am. A. 7 (12), 2169-2183 (1990)
10. P. Rizo, P. Grangeat, P. Sire, P. Lemasson, S. Delagenière, Proc. of the Materials Research Society of America fall meeting, Boston, MA, November 25 - December 1, (1990)
11. P. Grangeat, thèse de doctorat Ecole Nationale Supérieure des Télécommunications (1987)
12. P. Grangeat, Lecture notes in mathematics, Proc. of Conf. Mathematical Methods in Computed Tomography, G. T. Herman, A. K. Louis, F. Natterer, eds., Springer-Verlag, Berlin (1990)
13. A. A Kirillov, Soviet Math. Dokl. 2, 268-269 (1961)
14. P. Grangeat, P. Lemasson, P.Melennec, P. Sire, Proc. of Medical Imaging V, technical conference 1445: Image processing,San Jose, CA, Febuary 23-March 1srt, (1991)
15. P. Sire, P. Rizo, M. Martin, P. Grangeat, P. Morisseau, in these proceedings